

Colloidal hard dumbbells under gravity: structure and crystallization†

Matthieu Marechal and Marjolein Dijkstra*

Received 28th June 2010, Accepted 22nd August 2010

DOI: 10.1039/c0sm00589d

We study the structure and phase behavior of hard dumbbells under gravity. The fluid shows layering near the wall, where subsequent layers of dumbbells align alternately parallel or perpendicular to the wall. We observe coexistence of a fluid with a plastic crystal (PC) and an aligned crystal (CP1) in a single sediment for short dumbbells. For longer dumbbells, we observe a direct fluid–CP1 coexistence, while for dumbbells of almost tangent spheres, the aperiodic crystal phase appears in between the fluid and CP1 phase. The locations of the coexistences between these phases are well described by a simple expression based on an approximation similar to the local density approximation, which has been successfully applied to hard spheres under gravity [M. Marechal and M. Dijkstra, *Phys. Rev. E*, 2007, **75**, 061404]. The fluid–PC–CP1 coexistence could not be explained using this expression. We attribute this discrepancy to a lattice constant mismatch between the PC and CP1 phases. Finally, we show using direct simulations that the plastic crystal stacks preferably as the hexagonal close packed crystal for short dumbbells, as is the case for a bulk plastic crystal [M. Marechal and M. Dijkstra, *Phys. Rev. E*, 2008, **77**, 061405].

Introduction

The phase behavior of hard spheres in bulk, arguably the simplest system imaginable, is well understood by now. In particular, it was shown by computer simulations that such a system shows a purely entropy-driven phase transition from a disordered fluid phase to a face-centered-cubic (fcc) crystal phase at sufficiently high densities.^{1–3} Although the fcc phase is the most stable phase, the free energy difference with respect to the metastable hexagonal-close-packed (hcp) structure is only very small and is on the order of $10^{-3} k_B T$ per particle at the melting transition.⁴ Here we define k_B as Boltzmann's constant and T the absolute temperature. Historically, this system was mainly investigated as a model for simple atomic liquids. The advent of well controlled colloidal model systems has changed this. In fact, by screening the interactions between charged colloidal particles one can get interactions that are almost hard core-like. However, the effect of gravity is usually not negligible for colloids, since they are much larger than atoms. Hence, a spatial inhomogeneous suspension is obtained due to the gravitational field. The parameter that is associated with a gravitational field is the so-called gravitational length, which reads $\ell/g = (\beta m g \sigma)^{-1}$ where m is the effective or buoyant mass of the colloidal particles, $\beta = (k_B T)^{-1}$, σ the diameter of the colloids, and g the gravitational acceleration. Typically, ℓ/g is of the order of 10^{-1} – 10^3 for colloidal particles.

In a sediment, the local density increases with depth and (before equilibrium is reached) with time, which leads to crystallization when the pressure exceeds the freezing pressure of hard spheres. In fact, in colloidal systems, this is probably the

most widely used method to obtain crystals of micron-sized colloids.⁵ Crystallization in sedimentation profiles of hard spheres was studied using Monte Carlo simulations and density functional theory.^{6–12} The simulations in ref. 6 show a discontinuous transition where two layers crystallize at the same gravitational field strength. Upon increasing the gravitational field further, the crystalline film grows continuously. However, density functional theory predicts a discontinuous crystal growth *via* layering transitions upon increasing gravity in contrast with the simulation results.⁶ Our Monte Carlo simulations in ref. 12 supported the continuous layer-by-layer growth as found in the Monte Carlo simulations of Biben *et al.*⁶ Furthermore, we showed that the chemical potential μ at which the n th layer crystallizes can be obtained from

$$\mu - mgz'_n = \mu_{\text{coex}}, \quad (1)$$

where μ_{coex} is the chemical potential at bulk coexistence and z'_n is the height of layer n .

Having calculated the structure and phase behavior of hard spheres under gravity, one possible next step is to investigate a more complicated particle shape. Dijkstra and Savenko¹³ investigated the freezing transitions of hard rods under gravity for a $L/D = 5$, where L is the distance between the centers of the hemispherical end caps and D is the diameter of the cylinder. The authors find coexistence between up to four phases in a single sediment, a consequence of the rich phase diagram of hard rods, that features isotropic, nematic, smectic and crystal phases for this L/D . The phase coexistences were compared to a theoretical expression, that is similar to eqn (1). However, since the calculations were performed in the canonical ensemble, the equations feature the number of particles per unit area instead of the chemical potential μ .

While rods in the form of viruses^{14,15} are among the earliest colloidal systems to be studied, it is difficult to tune the aspect ratio of such systems. However, colloidal dumbbells can be

Soft Condensed Matter, Debye Institute for NanoMaterials Science, Utrecht University, Princetonplein 5, 3584 CC Utrecht, The Netherlands. E-mail: M.Dijkstra1@uu.nl

† This paper is part of a *Soft Matter* themed issue dedicated to the International Soft Matter Conference 2010.

synthesized that are monodisperse and whose aspect ratio can be easily tuned.^{16–18} In one of the possible synthesis methods, a layer of silica is grown around a pair of aggregated silica cores to obtain a dumbbell of length-to-diameter ratio $L^* = L/\sigma$, where L is the distance between the centers of the spheres and σ is the diameter of the spheres. Other synthesis methods also exist,^{17,18} but it is somewhat more difficult to tune the aspect ratio using these methods. Using dumbbells with a low aspect ratio $L^* \approx 0.3$, a plastic crystal was found experimentally¹⁹ above a packing fraction which corresponds reasonably well with the value at bulk coexistence as determined in ref. 20. At a very high packing fraction, even an aligned phase was found, although the authors have not investigated whether this is actually the aligned close packed crystal phase of hard dumbbells.²⁰ Peanut-shaped silica shells are shown to form a degenerate crystal, the two-dimensional equivalent of the a periodic crystal phase.^{18,21}

The bulk phase diagram of hard dumbbells was mapped out for a large part by Vega *et al.*^{20,22,23} and in ref. 24 we investigated the phase diagram for large L which features, aside from the aligned close packed crystal (CPI) also the aperiodic crystal phase, where each sphere of a dumbbell occupies one site of a hexagonal close-packed (hcp) or face-centered cubic lattice (fcc), but the dumbbells are otherwise randomly oriented. Furthermore, for small L we determined the type of plastic crystal: fcc or hcp by calculating free energy differences. In this paper we investigate the phase behavior of dumbbells under gravity. The phase diagram of dumbbells is similar to short spherocylinders especially for $L/\sigma \sim L/D \lesssim 0.6$.²³ Therefore we expect that the results presented here for dumbbells with $L \leq 0.6\sigma$, also apply quantitatively to short rods. The results for $L \geq 0.9\sigma$ certainly do not apply to rods, as spherocylinders do not order into an aperiodic crystal phase. In this paper, we show that at short L we obtain the expected fluid–plastic crystal–CPI coexistence, at intermediate L a direct fluid–CPI crystal coexistence and finally at large L a fluid–aperiodic crystal–CPI coexistence. Furthermore, we show that although the free energy difference between the fcc and the hcp plastic crystal is small, we can observe by direct simulations in gravity that the hcp phase is more stable for $L = 0.3\sigma$.

Model

We consider a system of hard dumbbells consisting of spheres of diameter σ . The center-to-center distance between the spheres is $L \leq \sigma$. Three values for $L/\sigma = 0.3, 0.6$ and 0.92 will be considered in this work, such that all gravity-induced phase coexistences that are possible according to the bulk phase diagram²⁴ can be found (there are three distinct possibilities). Furthermore, the values for L/σ were chosen such that the sediment contained a sizable number of layers of each possible phase at a certain value of L/σ for a chemical potential, which is not too high to prevent equilibration problems. We have briefly investigated a few other values of L and found no qualitative differences. We denote the center-of-mass position and the orientation of dumbbell i by \mathbf{r}_i and \mathbf{u}_i , respectively. The particles are subjected to a gravitational field oriented along the z -direction. In addition, the dumbbells are confined between two smooth hard parallel walls at $z = 0$ and $z = H$. In other words, the dumbbells are subjected to the external potential:

$$\phi(z_i, u_{i,z}) = \begin{cases} z_i - \frac{L}{2} |u_{i,z}| > \frac{\sigma}{2} & \text{and} \\ mgz_i & \\ z_i + \frac{L}{2} |u_{i,z}| < H - \frac{\sigma}{2} & \\ \infty & \text{otherwise} \end{cases} \quad (2)$$

where z_i is the vertical coordinate, $u_{i,z}$ is the z component of the direction vector of particle i , g is the gravitational acceleration and m the buoyant mass of the hard dumbbells. All simulations were performed at $mg\sigma/k_B T = 2$, so the gravitational length is equal to $\ell = \sigma/2$. The height H is chosen such that the number density of the centers of mass of the dumbbells $\rho_{\text{com}}(z)$ (see Sec.) at $z = H - \sigma/2$ is sufficiently small, *i.e.*, $\rho_{\text{com}}(H - \sigma/2)d^3 < 10^{-6}$, where d is the diameter of the sphere that has the same volume as a dumbbell and thus the system can be considered to be infinite in the z -direction. The lateral dimensions of the box are $L_x = a_0 n$ and $L_y = a_0 m\sqrt{3}/2$ with n, m integers. We choose n and m such that the lateral dimensions of the simulation box are nearly equal, which minimizes the finite-size effects for the fluid phase and still accommodates a hexagonal crystalline layer with lattice constant a_0 . To minimize finite size effects, relatively large horizontal box dimensions ($(n, m) = (14, 16)$) were required for $L = 0.3\sigma$, while for the dumbbells with larger aspect ratios ($L = 0.6\sigma$ and $L = 0.92\sigma$, smaller boxes could be employed ($(m, n) = (12, 14)$ and $(9, 10)$ respectively). The average number of particles in the simulations at the highest chemical potentials ranged from about 1500 for the smallest box size to almost 5000 for the $(14, 16)$ -system. The finite size effects were investigated by comparing order parameter profiles with profiles obtained for larger systems.

We employ periodic boundary conditions in the lateral dimensions in our simulations. Rather than fixing the number of particles we fix the chemical potential μ by adding standard²⁵ particle insertion and deletion moves to our Monte Carlo simulations. We define a dimensionless chemical potential by

$$\mu^* = \beta\mu - \log(V/\sigma^3) \quad (3)$$

where V is the thermal volume. This definition is such that the dimensionless ideal gas chemical potential equals $\log(N\sigma^3/V)$. Equilibration of the number of crystalline layers was rather slow. This is caused by the glassy behavior at high chemical potentials, which are necessarily above the chemical potential at bulk coexistence. We often needed simulation runs of over 10^7 successive Monte Carlo moves per particle to reach equilibration. Equilibration was checked by comparing order parameter profiles.

Initial configuration

In this paper, we only consider simulations that were initiated in one of two initial configurations. The first type of initial configuration is an empty simulation box ($N = 0$). In this case, the number of particles will increase slowly due to particle insertions and removals and initially the configuration of these particles will be fluid-like. When starting from such a fluid configuration, we never observed the CPI phase, which is the stable bulk phase at high pressures for all aspect ratios. The CPI phase must also be stable in gravity at high pressure, which corresponds to a large sediment, since it is the closest packed crystal phase. Therefore, the second initial configuration used in this work is a CPI crystal

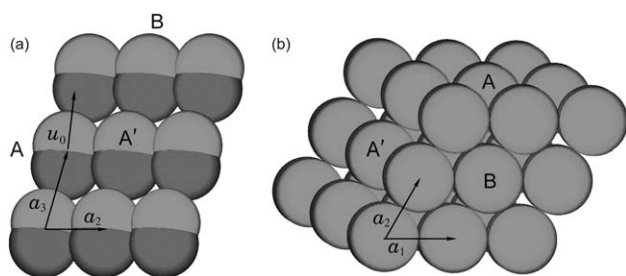


Fig. 1 The CP1 crystal, its lattice vectors, a_1 , a_2 and a_3 , and the direction vector of the dumbbells, u_0 . (a) Side view: \mathbf{a}_1 points into the plane of view. (b) Top view. The A face of the crystal is spanned by a_1 and a_3 ; the B face is spanned by a_1 and a_2 and the A' face, equivalent to the A face, is spanned by a_2 and a_3 . The A face is buckled *i.e.* one sphere of each dumbbell is closer to a plane spanned by a_1 and a_3 , than the other.

Table 1 The lattice parameters of CP1 at bulk coexistence as a function of L/σ

L/σ	a_0/σ	b_0/σ	c_0/σ	
0.3	1.08	0.538	1.14	18.8°
0.6	1.08	0.664	1.43	18.4°
0.92	1.05	0.917	1.65	30.3°

with the densest packed plane at the wall to minimize the gravitational energy. The densest plane of CP1 is the “B” plane, spanned by the lattice vectors \mathbf{a}_1 and \mathbf{a}_2 , see Fig. 1. The lattice vectors and the direction vector of CP1 are

$$\mathbf{a}_1 = (a_0, 0, 0), \quad \mathbf{a}_2 = \left(\frac{a_0}{2}, \frac{\sqrt{3}}{2}a_0, 0 \right), \quad (4)$$

$$\mathbf{a}_3 = \left(b_0, \frac{b_0}{\sqrt{3}}, c_0 \right), \quad \mathbf{u}_0 = \left(\frac{\sqrt{3}}{2} \sin \theta_0, \frac{\sin \theta_0}{2}, \cos \theta_0 \right), \quad (5)$$

where a_0 , b_0 and c_0 are lattice parameters and θ_0 is the angle between the z -axis and the equilibrium direction vector of the particles, \mathbf{u}_0 (see also Fig. 1). We have set these lattice parameters equal to the lattice parameters of CP1 at coexistence in bulk as listed in Table 1. We have also briefly considered CP1 crystals with the “A” plane aligned with the bottom wall, but we found that these crystals were less stable than the CP1 crystal with the “B” plane at the wall for all investigated L/σ . Since the layers are able to shift upwards and sideways due to the periodic boundary conditions, we expect that all lattice parameters except a_0 can be adjusted during the simulation. Whenever possible we started with the final configuration of a previous run, except when we consider the stability of hcp *versus* fcc of the plastic crystal phase.

Bond switch moves

The aperiodic crystal is a crystal of spheres that are connected into dumbbells (forming a “bond”) in a random fashion. Many different arrangements of such bonds (bond configurations) can occur as described in ref. 24. These arrangements are only strictly

degenerate at $L = \sigma$ and close packing *i.e.* only then the free energy of the dumbbells is the same for all bond configurations. As density and especially L is decreased, some of the arrangements become more frustrated than others by the fact that the bond length L between the spheres within a dumbbell is smaller than the distance between spheres of a neighboring dumbbell, which is equal to the lattice constant. For this reason when considering an aperiodic crystal at $L < \sigma$, it is paramount to implement a move which switches between bond configurations while preserving detailed balance. Such a bond switch move was introduced in ref. 24 in order to sample the different arrangements of bonds according to their local free energies and therefore correctly calculate the free energy of the aperiodic crystal in the bulk. To implement bond switch moves that preserve detailed balance and still work at finite density it was necessary to add single spheres to the simulation. In short, the bond switch move consists of two steps: First, we connect a non-bonded sphere to a sphere of a neighboring dumbbell and we cut the bond of that dumbbell, effectively moving the sphere from one lattice site in the aperiodic phase to another (for more details, see ref. 24). For bond switch moves in bulk, the diameter of the spheres was set to σ .

As the CP1 phase can be viewed as a deformed version of the fcc phase, it can transform into the aperiodic crystal phase using bond switch moves, provided that the layers can shift back to their positions in the fcc crystal phase. In our simulations in gravity, the top wall is far away so the layers can shift upwards, when the loss of gravitational energy is compensated by the gain in entropy due to the degeneracy of the aperiodic crystal. Furthermore, the periodic boundary conditions allow for a shift in the horizontal directions. We implemented the bond switch moves, as introduced in ref. 24, for dumbbells under gravity and observed a successful transformation from CP1 to the aperiodic crystal phase. There are a few differences between the implementation of bond switch moves in gravity and in bulk (see ref. 24), related to the (non-bonded) spheres that are required in order to be able to perform the bond switches. First, we subject the spheres to insertion and deletion moves and set their chemical potential to $\mu^*/2 - \Delta\mu^*$, where μ^* is the dimensionless chemical potential of the dumbbells and $\Delta\mu^* = 4$ ensures that the total fraction of single spheres is always small but nonzero. The (buoyant) mass m_s of the spheres was chosen to be half the mass of a dumbbell (m), while the diameters of the spheres (σ_s) was chosen such that the volume of a sphere is equal to half the volume of a dumbbell. In this way the internal mass densities of spheres and dumbbells are equal and separation of the dumbbells and the spheres by gravity should be minimal, according to Archimedes’ principle. Moreover, the acceptance ratio of the bond switch moves is higher if we move a smaller sphere, as the probability of creating overlaps with particles that are not involved in the move is lower.

Methods

In order to analyze our simulation results, we calculate two types of density profiles: One that measures the height distribution of the centers of mass of the dumbbells:

$$\rho_{\text{com}}^*(z) = \left\langle \frac{d^3}{A} \sum_i \delta(z - z_i) \right\rangle \quad (6)$$

and one that measures the height distribution of the individual spheres of each dumbbell:

$$\rho_{\text{sphere}}^*(z) = \left\langle \frac{d^3}{A} \sum_i \sum_{\eta} \delta(z - z_{i,\eta}) \right\rangle, \quad (7)$$

where d is the diameter of a sphere with the same volume as a dumbbell, which is given by $\frac{\pi}{6}(\sigma^3 + 3L\sigma^2/2 - L^3/2)$. The summation over i runs over all dumbbells and $\eta = \pm 1$ over the two spheres of each dumbbell. Similarly, all order parameter profiles can either be defined for the center-of-mass of the dumbbells or for the individual spheres of each dumbbell. To lighten the notation, we use the following definitions to abbreviate the averaging over the delta functions in the definitions of the order parameter profiles:

$$\langle A_i \rangle_{z,\text{com}} \equiv \langle \sum_i A_i \delta(z - z_i) \rangle / \langle \sum_i \delta(z - z_i) \rangle \quad (8)$$

and

$$\langle A_i \rangle_{z,\text{sphere}} \equiv \langle \sum_{i,\eta} A_{\{i,\eta\}} \delta(z - z_{i,\eta}) \rangle / \langle \sum_{i,\eta} \delta(z - z_{i,\eta}) \rangle, \quad (9)$$

where A_i is any measurable property of particle i and $A_{\{i,\eta\}}$ is a property of sphere $\eta = \pm 1$ of dumbbell i . To study the orientational order of the dumbbells, we measure the tensor

$$Q_{\alpha\beta}(z) = \left\langle \frac{3}{2} u_{i,\alpha} u_{i,\beta} - \frac{1}{2} \delta_{\alpha\beta} \right\rangle_{z,\text{com}}, \quad (10)$$

with $\alpha, \beta = x, y, z$. We use the zz component of $Q(z)$ to investigate the alignment along the z axis ($Q_{zz}(z) = 1$) or perpendicular to z ($Q_{zz} = -1/2$). We define the nematic order parameter at height z , $S_2(z)$, as the largest eigenvalue of $Q(z)$. For a fluid with a rotational symmetry of the director field around the z axis, as in the case of a fluid of dumbbells near a horizontal wall, one can show that Q is diagonal and that $Q_{xx} = Q_{yy} = -\frac{1}{2}Q_{zz}$. All dumbbells very close to the wall ($z_i \approx \sigma/2$) are oriented nearly parallel to the wall (otherwise they would overlap with the wall, see eqn (2)). Therefore, $S_2(\sigma/2) = Q_{xx}(\sigma/2) = Q_{yy}(\sigma/2) = -\frac{1}{2}Q_{zz}(\sigma/2) \approx \frac{1}{4}$. We use $S_2(z)$ to distinguish between the CPI phase ($S_2 \approx 1$) and the plastic crystal ($S_2 = 0$). We also define $S_2^{\text{sphere}}(z)$, that measures the orientational order of each dumbbell for which one of its spheres is located at height z , as the largest eigenvalue of

$$\left\langle \frac{3}{2} u_{i,\alpha} u_{i,\beta} - \frac{1}{2} \delta_{\alpha\beta} \right\rangle_{z,\text{sphere}}. \quad (11)$$

To determine crystallization, we measure the hexagonal bond order parameter of dumbbell $\gamma = i$ or sphere $\gamma = \{i, \eta\}$ using

$$\psi_{6,\gamma} = \frac{1}{N_\gamma} \sum_{\lambda=1}^{N_\gamma} \exp(i6\theta(\mathbf{r}_{\gamma\lambda})), \quad (12)$$

where the bond angle $\theta(\mathbf{r}_{\gamma\lambda})$ is defined as the angle between a reference axis and the center-of-mass displacement vector, $\mathbf{r}_{\gamma\lambda} = \mathbf{r}_\lambda - \mathbf{r}_\gamma$ and the sum over λ runs over the N_γ nearest neighbors of γ . A particle is defined as a neighbor, when

$$x_{\gamma\lambda}^2 + y_{\gamma\lambda}^2 + (4z_{\gamma\lambda})^2 < (1.4\sigma)^2, \quad (13)$$

where $x_{\gamma\lambda}$, $y_{\gamma\lambda}$ and $z_{\gamma\lambda}$ are the respective x , y and z components of $\mathbf{r}_{\gamma\lambda}$. This criterion is chosen in such a way, that the

neighbors γ are located primarily in the same layer as particle λ .

The center-of-mass hexagonal bond order parameter profile is defined as

$$\psi_6^{\text{com}}(z) = |\langle \psi_{6, i} \rangle_{z, \text{com}}|. \quad (14)$$

This parameter considers (virtual) bonds between the center-of-mass of a dumbbell and the centers of mass of its neighbors. It is 1 if the centers of mass of all dumbbells at height z are hexagonally ordered. Similarly, the hexagonal bond order parameter profile of the spheres is defined as

$$\psi_6^{\text{sphere}}(z) = |\langle \psi_{6, \{i, \eta\}} \rangle_{z, \text{sphere}}|. \quad (15)$$

In this case, bonds between sphere η of dumbbell i and neighboring spheres are considered. These neighbors can be part of another dumbbell or belong to the same dumbbell i . $\psi_6^{\text{sphere}}(z) = 1$ if the spheres of the dumbbells are perfectly hexagonally ordered.

In bulk systems of hard dumbbells, plastic crystals were found to be of either the fcc type or hcp type.²⁴ To distinguish between the two types of stacking we use the ψ_3 order parameter, which was used in ref. (26) to study defects in crystalline sediments of colloidal spheres. We require the local trigonal ordering in the layer above (+) or below (-) dumbbell i to define the trigonal bond order parameter ψ_3^\pm :

$$\psi_{3,i}^\pm = \frac{1}{N_\pm} \sum_j^{N_\pm} \exp(3i\theta(r_{ij})) \quad (16)$$

its horizontal distance to particle i is smaller than 1.1σ and its vertical distance is between 0.65σ and 1.4σ . If particle i is in a perfect fcc environment, $\psi_{3,i}^+ = -\psi_{3,i}^-$, while in an hcp environment $\psi_{3,i}^+ = \psi_{3,i}^-$. Accordingly, the ψ_3 profiles that are sensitive to hcp resp. fcc are defined as follows

$$\left. \begin{array}{l} \psi_3^{\text{hcp}}(z) \\ \psi_3^{\text{fcc}}(z) \end{array} \right\} = \left\langle \frac{1}{2} |\psi_{3,i}^+ \pm \psi_{3,i}^-| \right\rangle_{z,\text{com}}. \quad (17)$$

Results and discussion

Structure

We perform Monte Carlo simulations of a fluid of hard dumbbells with elongation $L = 0.3\sigma$, $L = 0.6\sigma$ and $L = 0.92\sigma$. Here and in the remainder of the paper we set the gravitational length ℓ to $\sigma/2$. We measure the dimensionless density profiles for the center-of-mass of the dumbbells, $\rho_{\text{com}}^*(z)$, and for the individual spheres of each dumbbell, $\rho_{\text{sphere}}^*(z)$ and the order parameter profile $Q_{zz}(z)$, that measures the alignment parallel ($Q_{zz}(z) = 1$) and perpendicular ($Q_{zz}(z) = -1/2$) to the z -axis. In Fig. 2, we show these profiles for $L = 0.3\sigma$ and $\mu^* = 20$, for $L = 0.6\sigma$ and $\mu^* = 40$ and for $L = 0.92\sigma$ and $\mu^* = 34$; these state points all lie just below the respective freezing transitions. From Fig. 2, we clearly observe pronounced layering in the density profiles, but the precise details depend heavily on L : For short dumbbells, the center-of-mass density profile resembles the density profiles obtained in sedimentation of hard spheres (with some effective diameter), while the first peak in the density profile of the

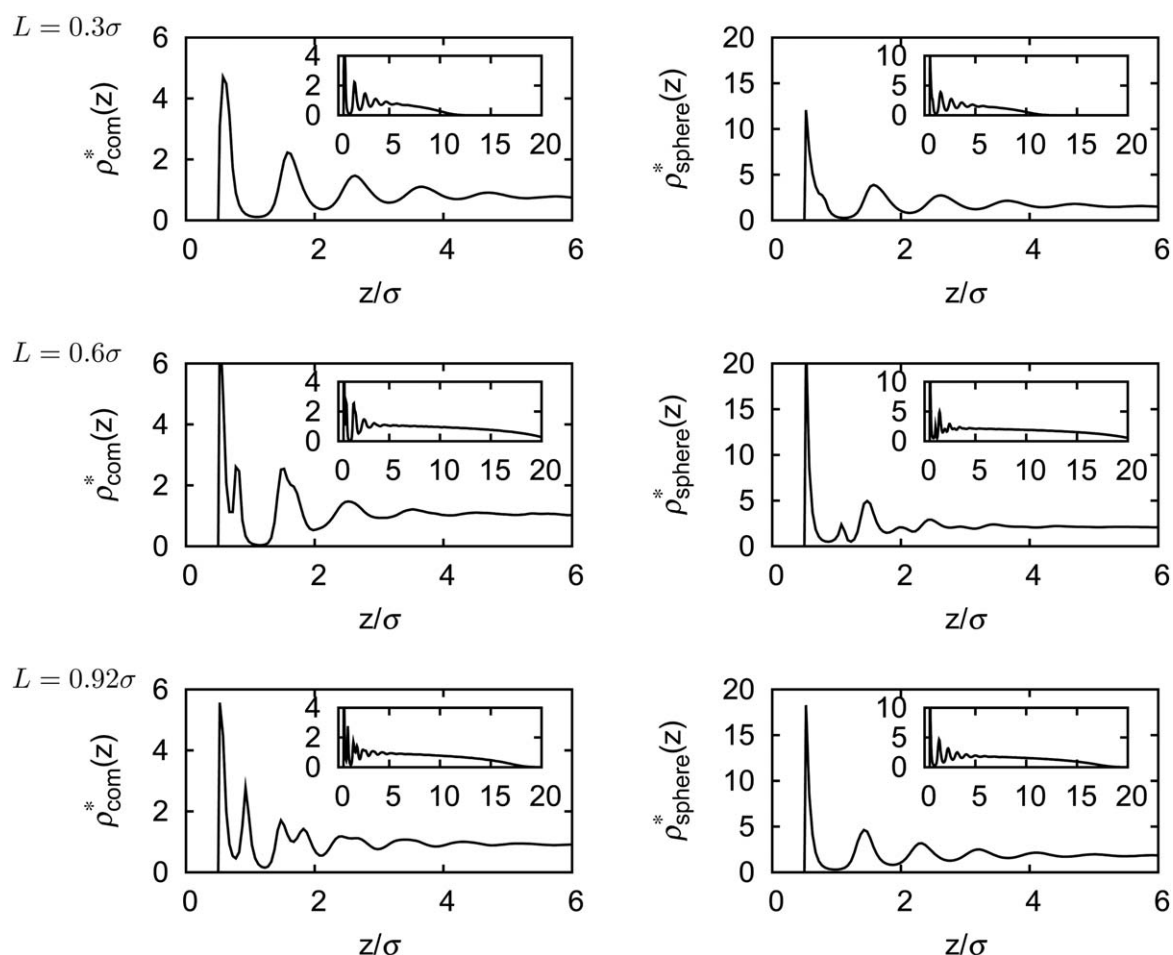


Fig. 2 Dimensionless density profiles for the center of mass of the dumbbells $\rho_{\text{com}}^*(z)$ and for the individual spheres of the dumbbells $\rho_{\text{sphere}}^*(z)$ of a fluid at $\mu^* = 20$ and $L = 0.3\sigma$ (top), $\mu^* = 40$ and $L = 0.6\sigma$ and $\mu^* = 34$ and $L = 0.92\sigma$ (bottom). The insets show the decay of the profiles over the full sediment.

individual spheres of each dumbbell has a small shoulder at $z = L + \sigma/2$ that corresponds to upright particles with $L = 0.3\sigma$. The $Q_{zz}(z)$ profile in Fig. 3, shows oscillations that seem to be out of phase with the oscillations in the density profile for the center of mass of dumbbells with 0.3σ . To be exact, there is a minimum in $Q_{zz}(z)$ at a slightly lower z -position than a maximum in $\rho_{\text{com}}^*(z)$ (corresponding to a vertical dashed line in Fig. 3), and also a maximum in $Q_{zz}(z)$ just below a minimum in $\rho_{\text{com}}^*(z)$. This is caused by the fact that upright dumbbells in layer n are shifted upwards compared to dumbbells that lie flat in the same layer due to the presence of the particles in layer $n - 1$ (or the wall for $n = 1$). For very long dumbbells ($L = 0.92\sigma$), the spheres of each dumbbell show the usual type of layering as shown in Fig. 2 (bottom row), while the center-of-mass profile has an unusual structure. We find density peaks in $\rho_{\text{com}}^*(z)$ at intermediate values of z *i.e.* $\frac{1}{2}(\sigma + L)$, $\frac{3}{2}(\sigma + L)$ *etc.* (the position of the wall is at $z = 0$ so the smallest possible z -position is $\sigma/2$). In addition, Fig. 2 shows that the layering in $\rho_{\text{com}}^*(z)$ correlates with the oscillations in $Q_{zz}(z)$ for $L = 0.92\sigma$. The odd numbered density peaks in $\rho_{\text{com}}^*(z)$ correspond to particles that are aligned on average perpendicular to z ($Q_{zz}(z) = -1/2$), while the even numbered layers are aligned parallel to z ($Q_{zz}(z) = 1$). This is caused by the

fact that dumbbells with each sphere in a different layer are aligned along z and have a center-of-mass position that is in between two layers of spheres, while dumbbells with both spheres in the same layer have their direction vector perpendicular to the z -axis and their center-of-mass z -position in a layer. For intermediate length $L = 0.6\sigma$, the dumbbells show a complicated behavior that shows aspects of both the short dumbbell and the long dumbbell profiles.

We also measure the density profiles and hexagonal order parameter profiles for crystalline sediments of hard dumbbells with the same elongations as for the fluid: $L/\sigma = 0.3, 0.6$ and 0.92 . As mentioned in the “Initial configuration” section, the initial configuration for these simulations is a CPI crystal with the hexagonal **B** plane spanned by \mathbf{a}_1 and \mathbf{a}_2 at the bottom wall. Fig. 4 shows the crystalline layers at the bottom of the sample, which can be seen from the negligible density in between the layers and the sharp peaks in the profiles. At $L = 0.3\sigma$ the center-of-mass profile shows well defined layers that are about σ apart for all heights. A small jump in the ψ_6 order parameter profile can be observed, which marks the transition from the CPI crystal at low z to the plastic crystal further up in the sediment. It can be seen from Fig. 4 that peaks in the density

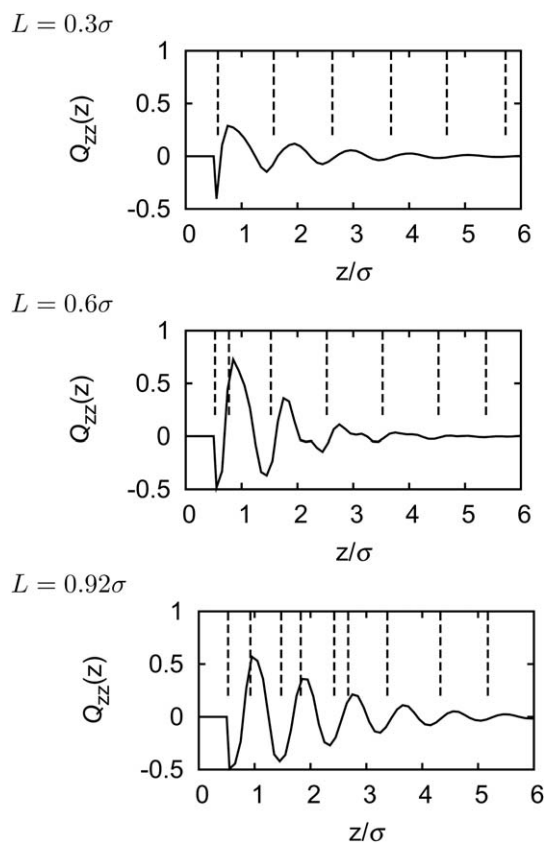


Fig. 3 Orientational order parameter profiles $Q_{zz}(z)$ of a fluid for the same parameters as in Fig. 2. The positions of the maxima of the center-of-mass density profiles, $\rho_{\text{com}}^*(z)$ (see Fig. 2) are indicated by vertical dashed lines.

profile of the plastic crystal (PC) are lower and less sharp, corresponding to larger fluctuations of the positions of the dumbbells. This also explains the slightly lower value of ψ_6^{com} for the plastic crystal. Finally, at high z , the density profile shows fluid-like behavior and ψ_6^{com} becomes very small, *i.e.* the plastic crystal is replaced by a fluid phase. A similar jump in the hexagonal order parameter profile of the spheres, $\psi_6^{\text{sphere}}(z)$, can be observed for $L = 0.92\sigma$, corresponding to the CP1 to aperiodic crystal transition. Here the $\rho_{\text{com}}^*(z)$ profile of the CP1 phase (only two layers of dumbbells) has an interlayer spacing of almost 2σ , while the aperiodic crystal peaks are separated by half the diameter. Half of the peaks of the aperiodic crystal phase are caused by the bonds which connect spheres within a layer of spheres and therefore the center of mass of the dumbbell is within the layer. The other half of the peaks is caused by inter-layer bonds. The center-of-mass profile of the aperiodic crystal phase looks rather ragged *i.e.* the peak heights differ, because the number of inter-layer bonds and the number of intra-layer bonds are not equal. For these reasons, it is more convenient to use the hexagonal order parameter profile for the individual spheres, rather than the hexagonal order parameter profile for the centers of mass of the dumbbells. The $\psi_6^{\text{spheres}}(z)$ profile shows pronounced ordering for both the CP1 and the aperiodic crystal phase for $L = 0.92\sigma$ as can be seen from Fig. 4. At high z , the aperiodic crystal phase is replaced by a fluid phase and ψ_6^{sphere} tends to zero. In conclusion, we find triphasic

coexistences both for small L and for large L , which is a consequence of the phase diagram of dumbbells compared to that of hard spheres. For small L , we find CP1–plastic crystal–fluid coexistence, while for large L a CP1–aperiodic crystal–fluid coexistence is observed. At the intermediate value of $L = 0.6\sigma$ we observed a sediment containing only the CP1 phase and the fluid phase, as expected from the bulk phase diagram of hard dumbbells.

Location and nature of the phase transitions

We investigated the fluid–crystal and crystal–crystal transitions, and calculated the locations of these transitions. We found that the hysteresis in the crystallization of the plastic and aperiodic crystals was lower than the spacing between μ^* values we considered. This can be explained by considering the melting of a crystal of which one or more of the surfaces is already exposed to a fluid phase, which usually shows little hysteresis also in the bulk *i.e.* the temperature or pressure at which melting first occurs in a simulation is the same as the thermodynamic melting point.^{27,28} In our simulations that include a gravitational force, the crystal is always in contact with a fluid layer and therefore one expects little hysteresis in the melting transition. As mentioned before, the CP1 phase did not form spontaneously, so the CP1 phase was used as an initial configuration and the melting behavior was studied to locate the transition. Therefore, also the hysteresis in this transition could not be determined. Possibly, the CP1 crystal did not form spontaneously in our simulations because of the slow dynamics at the large pressures at which it is stable in the bulk, which makes it difficult for the particles to align and form the CP1 crystal. Furthermore, the dumbbells in the first fluid or plastic crystal layer at the wall or on top of the CP1 phase lie parallel to the wall. These particles need to rotate upwards against gravity and the pressure of the particles on top of this layer to form a layer of CP1 crystal, which hinders the crystallization dramatically.²⁹ We have implemented molecular dynamics of slightly soft repulsive dumbbells to investigate whether the CP1 crystal would form in a system with realistic dynamics (as apposed to Monte Carlo moves). Unfortunately, also here the fluid did not crystallize into the CP1 phase. This leads to the conclusion that the CP1 crystal phase will not form spontaneously for repulsive dumbbells on time scales that can be investigated using current simulation techniques.

In addition to the order parameter profiles that are shown in Fig. 4, we also measured the nematic order parameter profile $S_2(z)$ for small L and the nematic order parameter profile $S_2^{\text{sphere}}(z)$ at the z -positions of the spheres for large L in order to distinguish between the different types of crystals (not shown in Fig. 4). We show the values of the relevant order parameters at the height of each layer as a function of μ in Fig. 5. We define the z -position of the n th layer, z_n , of the aperiodic crystal phase as the position of the n th maximum of $\rho_{\text{sphere}}^*(z)$, *i.e.* layer n is the n th layer of spheres for $L = 0.92\sigma$, while for $L = 0.3\sigma$ and $L = 0.6\sigma$ we number the layers of dumbbells *via* the maxima in the center-of-mass density profile, $\rho_{\text{com}}^*(z)$ and, correspondingly, z_n is the z -position of the n th maximum in the center-of-mass profile. We define layer n to be crystalline if $\psi_6(z_n)$ (left panel in Fig. 5) is larger than 0.5, while we define a crystalline layer to be CP1 if its crystalline and the orientational order parameter, $S_2(z_n)$ or

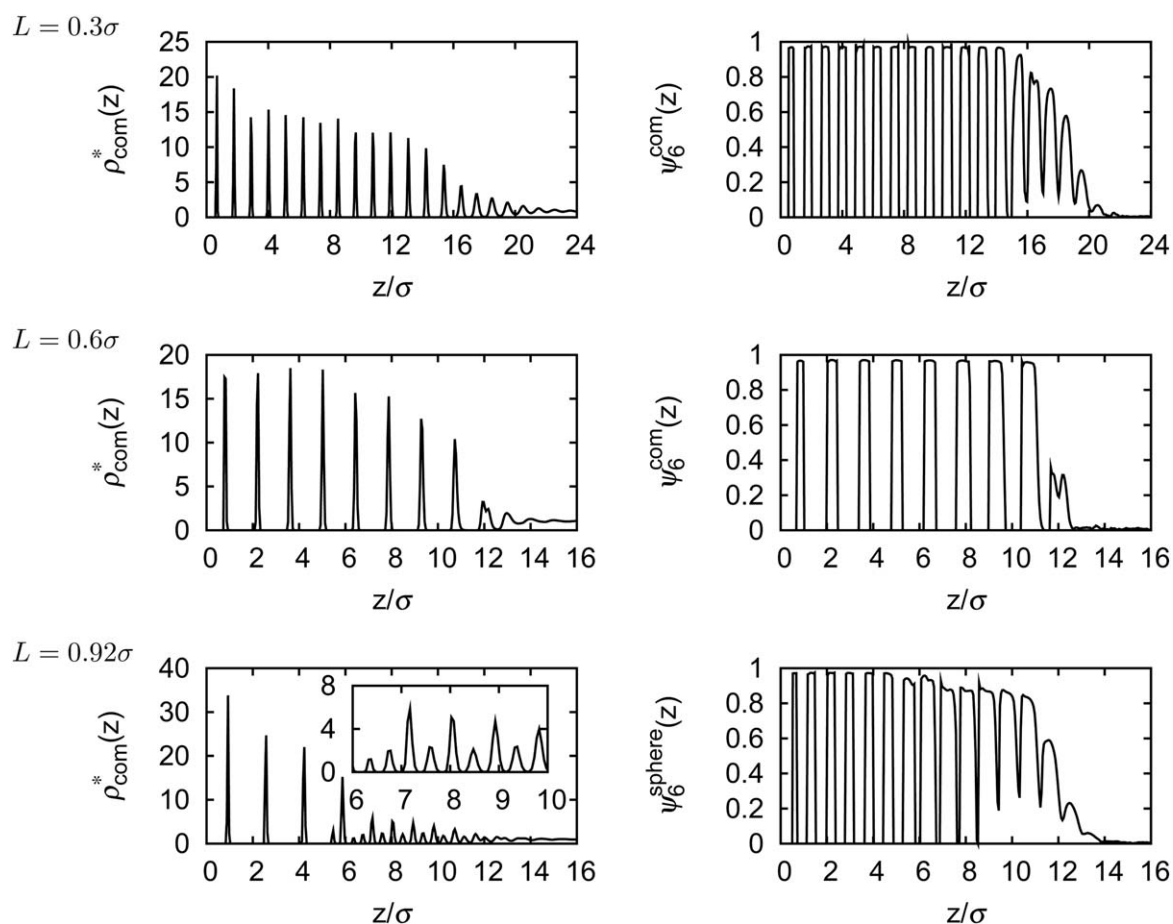


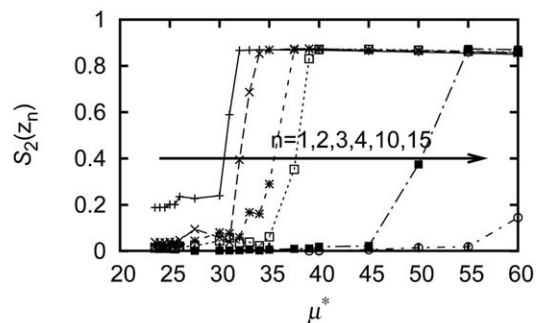
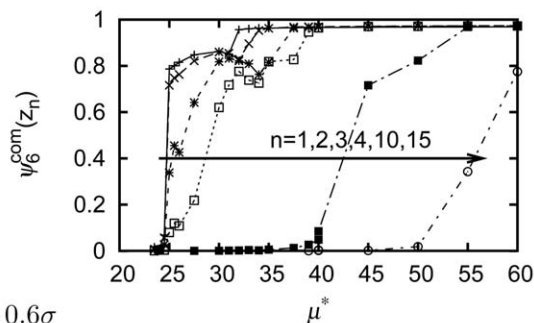
Fig. 4 Center-of-mass density profile $\rho_{\text{com}}^*(z)$ and hexagonal bond order parameter profile $\psi_6^{\text{com}}(z)$ for dumbbells with $L = 0.3\sigma$ at $\mu^* = 60$ (top row), and with $L = 0.6\sigma$ at $\mu^* = 60$ (middle row), the center-of-mass density profile $\rho_{\text{com}}^*(z)$ and hexagonal bond order parameter profile $\psi_6^{\text{sphere}}(z)$ of the individual spheres of dumbbells with $L = 0.92\sigma$ at $\mu^* = 60$ (bottom row). The inset in the bottom left plot is an enlargement of part of the $\rho_{\text{com}}^*(z)$ profile, showing oscillations with a period $\sim 0.5\sigma$ in the aperiodic crystal.

$S_2^{\text{sphere}}(z_n)$ (right panel in Fig. 5), is larger than 0.5. We will describe the sequences of transitions that occur when the chemical potential decreases (*i.e.* going from right to left in Fig. 5). As mentioned before, the particles in the bottom segment of the sediment form a CP1 crystal at high chemical potential for all three values of L considered, which is evident from Fig. 5 by the high values of the hexagonal bond order parameter $\psi_6(z_n) \approx 0.95$ and the nematic order (alignment) parameter $S_2(z_n) \approx 0.9$ for low n . As the chemical potential decreases, the thickness of the CP1 crystal decreases as the layers transform one by one into the lower density phase for the appropriate aspect ratio L . To be precise, the CP1 phase transforms into the plastic crystal phase for $L = 0.3\sigma$, the fluid phase for $L = 0.6\sigma$ and the aperiodic crystal phase for $L = 0.92\sigma$. During these transitions the particles lose their alignment *i.e.* $S_2(z_n)$ drops in the right panel of Fig. 5. Note, that the nematic order S_2 does not go to zero during these transitions, as the directors of the dumbbells directly on top of a crystal or the wall preferably lie in the horizontal plane, as discussed in the Methods section. Finally, the plastic crystal layers for $L = 0.3\sigma$ and the aperiodic layers for $L = 0.92\sigma$ melt (*i.e.* transform into a fluid) at yet lower chemical potential as indicated by a sudden decrease in $\psi_6(z_n)$ in Fig. 5 (left panel), when the chemical potential is decreased below the transition chemical potential for layer n .

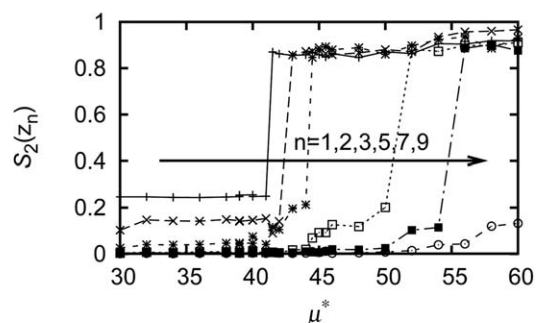
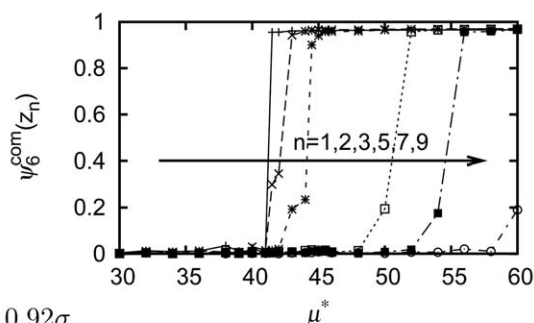
In ref. 12, we discussed the number of layers that first crystallizes for hard spheres in a gravitational field. Similarly, we count the number of layers n_{min} in the various crystals of dumbbells at the chemical potential just before they melted completely here. For the CP1 crystal phase of dumbbells with $L = 0.6\sigma$ and $L = 0.92\sigma$, n_{min} was one layer of dumbbells. The plastic crystal and CP1 phases of dumbbells with $L = 0.3\sigma$ consisted of 2 layers of dumbbells at the lowest chemical potential for which they were stable. Finally, $n_{\text{min}} = 2$ for the aperiodic phase of dumbbells with $L = 0.92\sigma$, where we counted layers of spheres instead of dumbbells for the aperiodic phase. For large L , a single layer of CP1 can be identified with two layers of spheres. So, in fact, the thinnest stable crystal of dumbbells for each L is about as thick as the thinnest stable of hard spheres¹² at the same gravitational length $g^* = \sigma/\ell = 2$, independent of the dumbbell aspect ratio L/σ .

From Fig. 5, it can be seen that the melting of layer $n = 1$ through n_{min} seems more discontinuous (it occurs between two closely spaced values of the chemical potential) than the melting of the other layers for most crystals (which occurs over a range of chemical potential values). The exception is CP1, which always seems to transform discontinuously into the lower density phase. Using a hand-waving argument, one can explain these results using the structure of the fluid layer, which lies directly on top of

$$L = 0.3\sigma$$



$$L = 0.6\sigma$$



$$L = 0.92\sigma$$

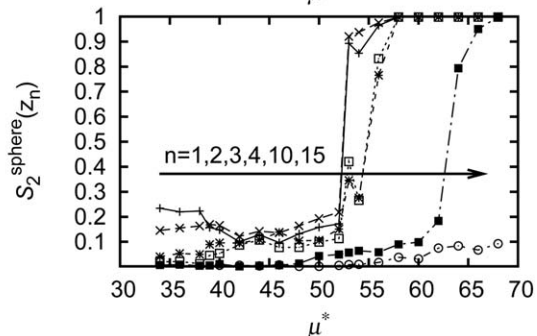
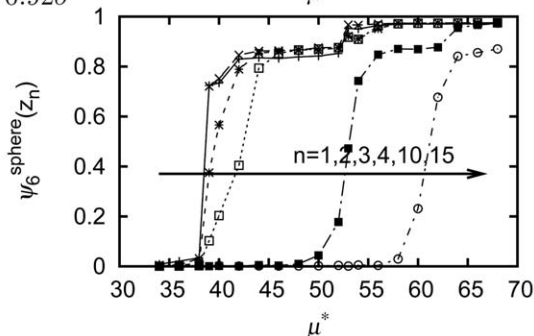


Fig. 5 Order parameters of the layer n as labeled as a function of reduced chemical potential μ^* . The order parameter of layer n is defined as the value of the corresponding order parameter profile at z_n , where z_n is defined as the n th maximum of $\rho_{\text{com}}^*(z)$ (top and middle row) or $\rho_{\text{spheres}}^*(z)$ (bottom row). Top: center-of-mass hexagonal bond order parameter $\psi_6^{\text{com}}(z_n)$ (left), nematic order parameter $S_2(z_n)$ (right) for $L = 0.3\sigma$. Middle: $\psi_6^{\text{com}}(z_n)$ (left) and $S_2(z_n)$ (right) for $L = 0.6\sigma$. Bottom: hexagonal bond order parameter $\psi_6^{\text{sphere}}(z_n)$ of the individual spheres of each dumbbell (left) and nematic order parameter profile at the z -positions of the spheres $S_2^{\text{sphere}}(z_n)$ (right) for $L = 0.92\sigma$. The order parameters of the first two layers for $L = 0.3\sigma$ and $L = 0.92\sigma$ and the third and fourth layer for $L = 0.92\sigma$ (primarily $S_2^{\text{sphere}}(z_n)$) are difficult to distinguish from each other, since these layers melt at the same chemical potential. For clarity, we do not show all layers.

the crystal. This fluid layer has some degree of hexagonal ordering, which can be appreciated from the nonzero value of the $\psi_6(z)$ profiles in Fig. 4. The same structuring is also observed for hard spheres and is caused by the top crystalline layer, that serves as a template. However, there is little directional alignment of the fluid layer. Therefore, in order to form a CPI layer on top of a already formed crystal the rotational symmetry of the direction vectors must be broken, while for the plastic crystal and the aperiodic crystal phase the hexagonally structured fluid can smoothly transform in a crystal phase. Typically, a transition that breaks a symmetry is discontinuous, which might explain the discontinuous growth of the CPI crystal. In the initial crystallization the translational symmetry is broken, since the fluid is not hexagonally ordered, and therefore we might expect this transition to be discontinuous. As a word of caution, we note that the same reasoning can be applied to the freezing of two-dimensional

hard discs, which is currently thought to occur through two second order transitions.^{30–32}

Comparison to bulk

The reduced chemical potentials at which the transitions (or the disappearance of a phase in the sediment) occur μ_{trans}^* are compared to the bulk coexistence chemical potentials in Fig. 6 and Tab. 2. Since we require the chemical potential at the coexistence between the fluid and aperiodic phases and the coexistence between the aperiodic and CPI phases and these were not calculated in our earlier paper on the bulk phase behavior of hard dumbbells,²⁴ we repeated the bulk free energy calculations and common tangent constructions for $L = 0.92\sigma$ using simulations that employ bond switch moves (see ref. 24 for full details). For completeness, we also list the resulting coexistence densities and pressures in Tab. 3.

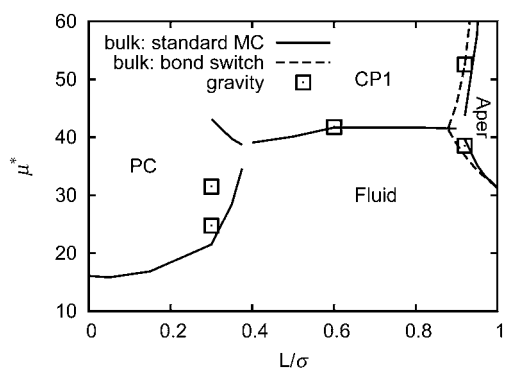


Fig. 6 Bulk phase diagram for hard dumbbells in the μ^* - L/σ representation, where μ^* is the dimensionless bulk chemical potential as defined in eqn (3) and the results indicated by the solid lines are obtained in standard Monte Carlo simulations without special moves, while bond switch moves were employed for the results indicated by the dashed lines. The squares denote the dimensionless chemical potentials (μ^*) at which the phase transitions occur in a gravitational field with $\ell = \sigma/2$. Fluid denotes the fluid phase, PC denotes the plastic crystal phase, CP1 the periodic crystal and Aperi the aperiodic crystal phase.

Table 2 The phases found in our simulations for hard dumbbells with center-to-center distance to diameter ratio (L/σ), the lowest chemical potential at which they were found (μ_{trans}^*), the chemical potential of the coexistence between the phase of interest and the phase at lower density (see Fig. 6) and the thickness of the layers Δz . For $L = 0.92\sigma$, Δz is the thickness of a layer of spheres, while for $L = 0.3\sigma$ and $L = 0.6\sigma$ Δz is the thickness of a layer of dumbbells

L/σ	phase	μ_{trans}^*	μ_{coex}^*	$\Delta z/\sigma$
0.3	PC	24.75 ± 0.25	21.50	1.14
0.3	CP1	31.5 ± 0.5	43.12	1.13
0.6	CP1	41.75 ± 0.25	41.66	1.42
0.92	aper	38.5 ± 0.5	34.25	0.83
0.92	CP1	52.75 ± 0.25	52.46	0.78

Table 3 Reduced densities, pressures and chemical potentials of the bulk fluid-aperiodic crystal and aperiodic crystal-CP1 coexistences at various $L = 0.92\sigma$ as calculated using simulations that include bond switch moves.²⁴ The unit of length used in the definition of the dimensionless density and pressure is the diameter of a sphere with the same volume as a dumbbell with aspect ratio $L = 0.92\sigma$

Phase 1	Phase 2	$\rho_1 d^3$	$\rho_2 d^3$	$\beta P d^3$	μ^*
fluid	aper	1.042	1.124	30.01	34.25
aper	CP1	1.217	1.255	48.46	52.46

For $L = 0.6\sigma$ and $L = 0.92\sigma$, μ_{trans}^* corresponds nicely to the bulk values, which gives confidence in the equilibration. However, for $L = 0.3\sigma$ the PC-CP1 freezing transition is far off. To investigate this discrepancy, we investigate the structure of a fluid-PC-CP1 sediment at $\mu^* = 35$, where we did not expect to find any stable CP1 crystal phase.

From the structure of one layer of the plastic crystal we observe that the lattice direction of the plastic crystal conforms to that of the CP1 phase and to the simulation box. Furthermore, we find that the PC layer in contact with the CP1 crystal has

a horizontal lattice constant of about 1.18σ , which is significantly smaller than the lattice constant of the bulk plastic crystal at the PC-CP1 coexistence, which is about 1.2σ . The other layers of the plastic crystal phase have a lattice constant of about 1.24σ , similar to the lattice constant in the bulk at the fluid-PC coexistence.

We investigated the reproducibility of these unexpected results at a dimensionless chemical potential $\mu^* = 35$. When the simulation was allowed to run for ten times longer than the rest of the runs, the number of crystalline layers and the lattice constants of the crystals in the sediment were the same as for the shorter simulations. The presence of an intermediate layer of plastic crystal with a lattice constant of $\sim 1.18\sigma$ in between the CP1 crystal and the other, the plastic crystal with lattice constant of $\sim 1.24\sigma$ were also reproduced for a larger horizontal box size corresponding with 20×20 particles in a layer of the CP1 crystal and also for a larger gravitational length $\ell = \sigma$. The differences between all density and order parameter profiles of the larger system and the corresponding profiles of the original (14, 16) system were smaller than the statistical error. The z -positions of the plastic crystal-CP1 and fluid-plastic crystal for $\ell = \sigma$ also corresponded nicely to the results for $\ell = \sigma/2$, i.e. z/ℓ was the same for both values of ℓ . This reproducibility, suggests that the observed structure holds rather generally for the PC-CP1 interface.

Using these results, our explanation for the discrepancy between the locations of the PC-CP1 coexistence as expected from bulk simulations and as observed in our simulations in gravity is as follows. When the CP1 phase partially melts in the presence of a gravitational field, the remaining CP1 layers form a template on top of which the plastic crystal (PC) grows. Unfortunately, the hexagonal face of CP1 is a rather poor template for the formation of a plastic crystal, since the (horizontal) lattice constant of CP1 is considerably smaller than the lattice constant of the plastic crystal (about ten percent at bulk coexistence between the two phases). To cope with this poor template, a defect-rich, high density plastic crystal layer grows directly on top of the CP1 crystal, followed by the remainder of the plastic crystal with a lower density. Because of the defects and the high density (which is higher than the bulk crystal) the intermediate layer has a higher local free energy (or grand potential) than the bulk plastic crystal, which explains why the topmost CP1 layer transforms into this defect-rich layer at a lower chemical potential than expected from bulk coexistence. A second scenario is that the high density in the intermediate layer hinders diffusion upwards out of the CP1 crystal and therefore kinetically hinders the melting of the CP1 crystal. We cannot exclude this alternative scenario, although we have run very long simulations to ensure that our simulations are equilibrated. Regardless of which scenario holds, we expect from the results at the other values of L that the CP1 crystal is metastable at chemical potentials below bulk coexistence *i.e.* that the defect-rich layer only forms a barrier for the complete melting of the CP1 crystal.

The number of layers as a function of chemical potential

Now, we compare our results for the freezing of the n th layer with the estimate that layer n crystallizes when

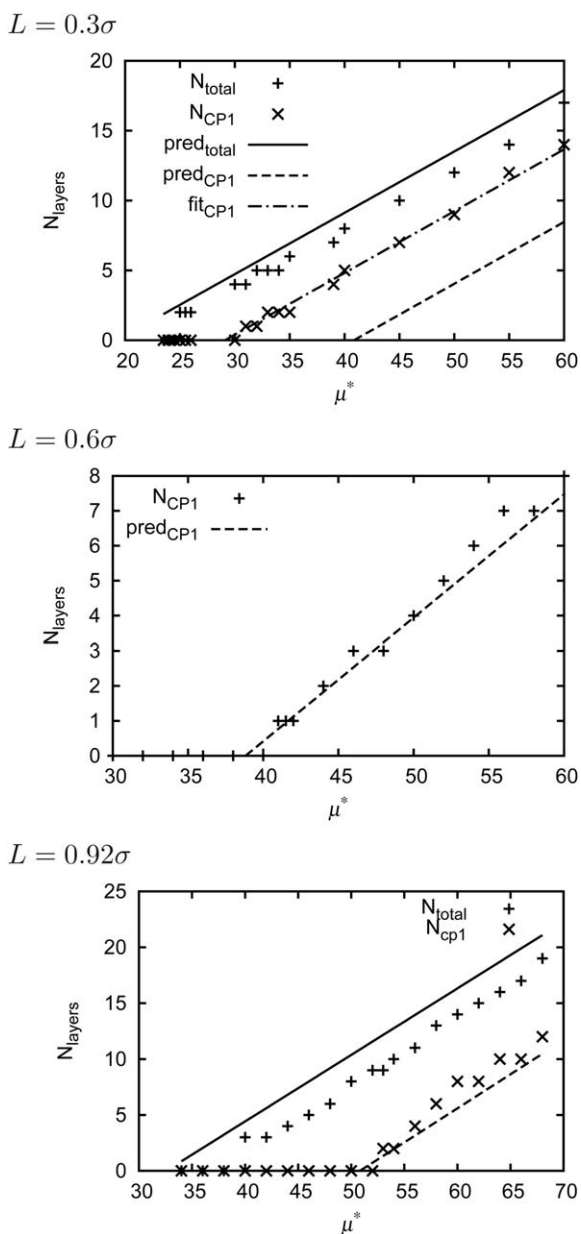


Fig. 7 The number of CP1 crystalline layers N_{CP1} and the total number of crystalline layers N_{total} as a function of dimensionless chemical potential μ^* for (from top to bottom) $L = 0.3\sigma$, 0.6σ and 0.92σ . The lines labeled by “pred” denote our prediction (13) based on the chemical potential at bulk coexistence, while “fit” denotes a fit (see text).

$$\mu - mgz_n = \mu_{\text{coex}} \quad (18)$$

where μ_{coex} is the chemical potential at bulk coexistence and $z_n = \Delta z(n - 1)$, where Δz is the thickness of a layer. According to this definition, z_n is the z -position in between layer n and $n - 1$. The thickness Δz is obtained from a fit of z_k as a function of the number of crystalline layers (N_{layers}), where k is the top layer of the crystal of interest. The resulting layer thicknesses are tabulated in Tab. 2. Note that for the plastic crystal and the aperiodic crystal phase, k is not equal to N_{layers} , when there are also layers of the CP1 crystal phase present in the sediment. The expression for the chemical potential at which the k th layer crystallizes, eqn

(18) for $n = k$, can be inverted to obtain the number of crystalline layers as a function of μ :

$$N_{\text{layers}}(\mu) = \lfloor (\mu - \mu_{\text{coex}}) / (mg\Delta z) \rfloor + 1, \quad (19)$$

where $\lfloor x \rfloor$ is the largest integer smaller than x . The number of crystalline layers and the prediction (13) are plotted in Fig. 7. As before, we plot the number of layers of spheres in Fig. 7 for $L = 0.92\sigma$, while for the other values of L we plot the number of dumbbell layers.

The agreement between prediction (13) and the data is reasonable except for $L = 0.3\sigma$. Furthermore, the slope is correctly predicted for all L . For $L = 0.3\sigma$, the number of layers of CP1 (N_{CP1}) is similarly affected by the mismatch between the plastic crystal lattice and the CP1 lattice as the PC–CP1 transition itself: the bottom layer of the plastic crystal phase is destabilized, when in contact with the CP1 phase (see the discussion at the end of the previous section). To quantify the discrepancy between the prediction and the simulation results, we fit eqn (19) to N_{CP1} with μ_{coex}^* as the only fit parameter; the result for the chemical potential μ_{coex}^* was 31.4, while the reduced chemical potential at bulk PC–CP1 coexistence is 43.12. It should be noted, that eqn (19) with adjusted μ_{coex}^* might not give the correct result for other values of the gravitational length ℓ .

Relation to experiments on colloids

In experiments, the chemical potential is usually not readily available, although it has been obtained in a (mass) density matched suspension in ref. 33 using a variant of the Widom particle insertion method.³⁴ However, the pressure can be easily obtained by integrating the density profile from the ideal gas at the top of the sediment to the height of interest. We checked for the center-of-mass profile of dumbbells and for $\rho_{\text{sphere}}^*(z)/2$ that the pressure at height z obtained by this integration oscillates around the bulk pressure that corresponds to the chemical potential $\mu - mgz$. These unavoidable oscillations are caused by the layering, but we noticed that the pressure at the peak of the density profile, as well as the pressure right in the middle between two layers, $P(z'_n)$, corresponds almost exactly to the bulk pressure at those heights. This is a nontrivial result, since the gravitational field is rather strong ($\ell/\sigma = 0.5$). Using this result, we find that layer n is crystalline, when the pressure $P(z'_n)$ in between layers n and $n - 1$ is higher than the bulk coexistence pressure. In the case of CP1 at $L = 0.3\sigma$, the fitted $\mu_{\text{coex}}^* = 31.4$ can be inserted in eqn (18) to obtain the chemical potential at which a layer crystallizes. As mentioned, this chemical potential is much lower than the chemical potential at bulk PC–CP1 coexistence, therefore we have no bulk pressure data at this chemical potential. Instead, we use the local pressure $P(z'_n)$ as a function of the local chemical potential $\mu(z'_n) = \mu - mgz'_n$ in our sediment, which results in a dimensionless pressure $d^3P(z)/k_B T \approx 27$ at $\mu^*(z) = 31.4$. Finally, we predict that layer n will be crystalline when,

$$P(z'_n) > P_0, \quad (20)$$

where P_0 is equal to the coexistence pressure (see ref. 24, ref. 20, 22, and 23 and Table 3), except for the PC–CP1 transition at $L = 0.3\sigma$ where $d^3P_0/k_B T \approx 27$.

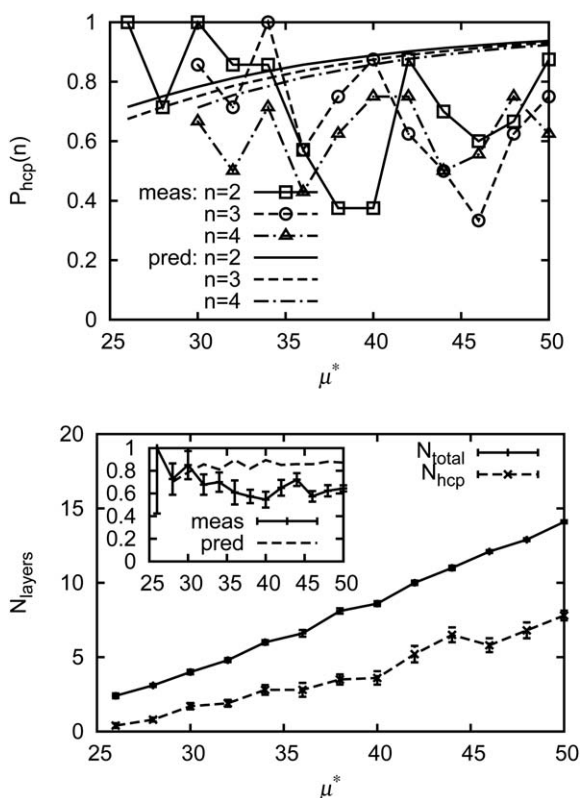


Fig. 8 Top: Probability to find an hcp layer P_{hcp} as measured using $\psi_3(z_n)$ (symbols), and as predicted by eqn (22) (smooth lines). Bottom: number of hcp layers N_{hcp} and total number of crystalline layers N_{total} ; inset: $N_{\text{hcp}}/(N_{\text{fcc}} + N_{\text{hcp}})$ as measured and as predicted by eqn (23). The stacking of the top and bottom layer is undefined, so $N_{\text{fcc}} + N_{\text{hcp}} = N_{\text{total}} - 2$.

We must also estimate whether the free energy barriers or kinetic hindrance that impaired the crystallization of CP1 for $L/\sigma = 0.3$ and 0.6 and the melting of CP1 at chemical potentials above $\mu = 31.4$ for $L/\sigma = 0.3$ are as insurmountable in experiments as in our simulations. We will do so by a crude order of magnitude comparison of the accessible time scales in experiments and simulations by the free (self) diffusion time τ_D . Only if the time available for the typical experiment in diffusion units is much larger than the “time” available in our Monte Carlo simulations, the experiments can be expected to give very different results. For micron-sized colloids τ_D is usually around a few seconds,³⁵ while τ_D is around a few milliseconds of wall clock time in our simulations for our largest system sizes. According to this crude comparison of time scales, our longest simulation, that ran for one week, corresponds to an experiment of many years. Therefore, it seems likely that the free energy barriers that we encountered during our simulations will not be overcome in experiments of micron-sized repulsive dumbbells.

Plastic crystal: hcp or fcc?

The dumbbells in the plastic crystal can either reside on an hcp lattice or an fcc lattice. The free energy difference between these two phases in bulk is small ($\leq 0.01k_B T$ per particle²⁴), but still much larger than the free energy difference between the fcc and hcp phases of hard spheres (difference is of order $10^{-3}k_B T$ per

particle⁴). Furthermore, the stable phase for dumbbells of any appreciable aspect ratio ($L > 0.1\sigma$) is hcp, while the stable phase for hard spheres is fcc. We investigated whether the small free energy difference between the two types of plastic crystals can be observed in a spontaneously crystallized sediment *i.e.* starting from a fluid phase. We initiated all runs with zero particles; the number of particles slowly increases during the simulation in the grand canonical ensemble due to the insertion moves. In this case, it is advantageous that the CP1 phase never forms spontaneously, as it allows us to investigate higher chemical potentials than the plastic crystal–CP1 coexistence. In Fig. 8 we show the probability to find an hcp layer as obtained from $\psi_3^{\text{hcp}}/(\psi_3^{\text{fcc}} + \psi_3^{\text{hcp}})$ for layers $n = 2, 3$ and 4 for hard dumbbells with $L = 0.3\sigma$ and gravitational length $\ell = \sigma/2$. We ran 10 simulations at each chemical potential, therefore the measured probabilities are multiples of 0.1 . We indeed find that the probability to find an hcp layer is higher than the probability to find an fcc layer, although for higher chemical potentials the data is rather noisy because of the slow equilibration at high pressure. Using the bulk free energy differences between hcp and fcc for hard dumbbells as determined in ref. 24, one can estimate the probability to find an hcp layer in the bulk. The probability that one layer in the bulk, consisting of N_l particles, is hcp stacked is given by

$$P_{\text{hcp}}(\rho) = \frac{\exp(-\beta N_l f_{\text{hcp}})}{\exp(-\beta N_l f_{\text{hcp}}) + \exp(-\beta N_l f_{\text{fcc}})}, \quad (21)$$

where $f \equiv F/N$ is the bulk free energy per particle, and where the surface tension between fcc and hcp (which is only known for hard spheres³⁶) is ignored. Furthermore, we do not consider grain boundaries or other defects within a layer, since these were never observed in our simulations. This has the effects that a layer is always either completely hcp or fcc stacked. We fit $\Delta f(\rho) = (F_{\text{fcc}} - F_{\text{hcp}})/N$ to the bulk free energy difference as a function of ρ and L . For $L = 0.3\sigma$ it is always positive and of order $0.01k_B T$ per particle. Subsequently, we fit the density as a function of the chemical potential in the bulk, $\rho(\mu)$, and make use of a variant of the local density approximation³⁷ to write

$$P_{\text{hcp}}(z_n) = 1/[1 + \exp(\beta N_l \Delta f(\rho(\mu - mgz_n)))] \quad (22)$$

where $N_l = 124$ is the number of particles in a single layer. We plot this expression along with our simulation results in Fig. 8. Although the dependence on μ and the layer number can not be confirmed by our data, we see that for low μ our simulation results agree roughly with the theoretical prediction. In Fig. 8 we also show the number of hcp stacked layers, N_{hcp} along with the total number of crystalline layers N_{total} and, in the inset, the ratio of the N_{hcp} over the total number of crystalline layers for which the stacking can be defined, *i.e.* $N_{\text{total}} - 2$. Similarly as described above, the average number of layers that are hcp stacked can be calculated using the bulk free energy:

$$\langle N_{\text{hcp}} \rangle = \frac{\sum_{\{s_n\}} \sum_n s_n \exp(+\beta \sum_n s_n \Delta F_n)}{\sum_{\{s_n\}} \exp(+\beta \sum_n s_n \Delta F_n)} \quad (23)$$

where n denotes the n th layer, s_n denotes the stacking of layer n : $s_n = 1$ if the layer is hcp stacked, $s_n = 0$ if the layers is fcc stacked, $\{s_n\}$ is a particular stacking configuration, such that the sum over $\{s_n\}$ is over all possible stacking configurations and

finally $\Delta F_n = N_l \Delta f(\rho(\mu - mgz_n))$. This sum can be calculated explicitly because the number of layers is not very large. From the inset of Fig. 8, we see that expression (17) overestimates the actual number of layers, except at low chemical potential. We attribute this discrepancy to the noise due to slow thermalization, which tends to randomize the stacking *i.e.* bring the stacking probability closer to 0.5.

Conclusion

We investigated the structure and phase behavior of hard dumbbells in a gravitational field. The structure of the fluid is influenced by the presence of the hard wall showing oscillations not only in the density profile but also in the orientational order profile. The structure of the crystal is not very sensitive to the effect of the gravitational field as the dumbbells in a crystal are already layered. An interesting effect of a gravitational field for particles that have more than one crystal phase is that coexistences can be observed between more than two phases, in this case between the fluid, plastic crystal and aligned crystal phases for short dumbbells and the fluid, aperiodic crystal and aligned crystal phases for long dumbbells. The locations of the interfaces between the various phases in a gravitational field are usually well described by comparing local chemical potentials (or pressures) to the bulk coexistence state points, although special care must be taken when considering the phase transformation between two crystals with mutually incompatible structures. This is an interesting and surprising result, because we are considering gravitational lengths of the order of the diameter of the particle, for which the local density approximation is assumed to be invalid. Here, the local density approximation refers to the assumption that the free energy of a slab at a certain height is equal to the bulk free energy with the bulk density replaced by the local density in the slab.³⁷ Finally, we showed that the free energy difference between the fcc and the hcp type of the plastic crystal of hard dumbbells results in a directly observable preference for hcp in a sediment of hard dumbbells.

Acknowledgements

Financial support is acknowledged from an NWO-VICI grant and from the High Potential Programme of Utrecht University. We also thank A. van Blaaderen and F. A. Demirörs for stimulating discussions.

References

- 1 W. W. Wood and J. D. Jacobson, *J. Chem. Phys.*, 1957, **27**, 1207.
- 2 B. J. Alder and T. E. Wainwright, *J. Chem. Phys.*, 1957, **27**, 1208.
- 3 W. G. Hoover and F. H. Ree, *J. Chem. Phys.*, 1968, **49**, 3609.
- 4 P. G. Bolhuis, D. Frenkel, S. C. Mau and D. A. Huse, *Nature*, 1997, **388**, 235.
- 5 J. P. Hoogenboom, P. Vergeer and A. van Blaaderen, *J. Chem. Phys.*, 2003, **119**, 3371.
- 6 T. Biben, R. Ohnesorge and H. Löwen, *Europhys. Lett.*, 1994, **28**, 665.
- 7 D. C. Hong, *Phys. A*, 1999, **271**, 192.
- 8 J. A. Both and D. C. Hong, *Phys. Rev. E: Stat., Nonlinear, Soft Matter Phys.*, 2001, **64**, 061105.
- 9 W. Nuesser and H. Versmold, *Mol. Phys.*, 1999, **96**, 893.
- 10 A. Mori, S.-i. Yanagiya, Y. Suzuki, T. Sawada and K. Ito, *J. Chem. Phys.*, 2006, **124**, 174507.
- 11 S. C. Kim and S. H. Suh, *J. Phys.: Condens. Matter*, 2003, **15**, 6617.
- 12 M. Marechal and M. Dijkstra, *Phys. Rev. E: Stat., Nonlinear, Soft Matter Phys.*, 2007, **75**, 061404.
- 13 S. V. Savenko and M. Dijkstra, *Phys. Rev. E: Stat., Nonlinear, Soft Matter Phys.*, 2004, **70**, 051401.
- 14 J. D. Bernal and I. Fankuchen, *J. Gen. Physiol.*, 1941, **25**, 111.
- 15 S. Fraden, G. Maret, D. L. D. Caspar and R. B. Meyer, *Phys. Rev. Lett.*, 1989, **63**, 2068.
- 16 P. M. Johnson, C. M. van Kats and A. van Blaaderen, *Langmuir*, 2005, **21**, 11510.
- 17 E. B. Mock, H. De Bruyn, B. S. Hawkett, R. G. Gilbert and C. F. Zukoski, *Langmuir*, 2006, **22**, 4037.
- 18 S. H. Lee, S. J. Gerbodea, B. S. John, A. K. Wolfgang, F. A. Escobedo, I. Cohen and C. M. Liddell, *J. Mater. Chem.*, 2008, **18**, 4881.
- 19 E. B. Mock and C. F. Zukoski, *Langmuir*, 2007, **23**, 8760.
- 20 C. Vega, E. P. A. Paras and P. A. Monson, *J. Chem. Phys.*, 1992, **96**, 9060.
- 21 S. J. Gerbode, S. H. Lee, C. M. Liddell and I. Cohen, *Phys. Rev. Lett.*, 2008, **101**, 058302.
- 22 C. Vega, E. P. A. Paras and P. A. Monson, *J. Chem. Phys.*, 1992, **97**, 8543.
- 23 C. Vega and P. A. Monson, *J. Chem. Phys.*, 1997, **107**, 2696.
- 24 M. Marechal and M. Dijkstra, *Phys. Rev. E*, 2008, **77**(061405).
- 25 D. Frenkel and B. Smit, *Understanding molecular simulation* (Academic Press, 2002).
- 26 J.-M. Meijer, V. W. A. de Villeneuve and A. V. Petukhov, *Langmuir*, 2007, **23**, 3554.
- 27 S. R. Phillpot, J. F. Lutsko, D. Wolf and S. Yip, *Phys. Rev. B: Condens. Matter*, 1989, **40**, 2831.
- 28 E. G. Noya, C. Vega and E. de Miguel, *J. Chem. Phys.*, 2008, **128**, 154507.
- 29 T. Schilling and D. Frenkel, *Phys. Rev. Lett.*, 2004, **92**, 085505.
- 30 A. Jaster, *Phys. Rev. E: Stat. Phys., Plasmas, Fluids, Relat. Interdiscip. Top.*, 1999, **59**, 2594.
- 31 S. Sengupta, P. Nielaba and K. Binder, *Phys. Rev. E: Stat. Phys., Plasmas, Fluids, Relat. Interdiscip. Top.*, 2000, **61**, 6294.
- 32 A. Jaster, *Phys. Lett. A*, 2004, **330**, 120.
- 33 R. P. A. Dullens, D. G. A. L. Aarts and W. K. Kegel, *Proc. Natl. Acad. Sci. U. S. A.*, 2006, **103**, 529.
- 34 B. Widom and J. Chem. Phys., 1963, **39**, 2808.
- 35 A. van Blaaderen, J. Peetermans, G. Maret and J. K. G. Dhont, *J. Chem. Phys.*, 1992, **96**, 4591.
- 36 S. Pronk and D. Frenkel, *J. Chem. Phys.*, 1999, **110**, 4589.
- 37 R. Evans, in *Fundamentals of Inhomogeneous Fluids*, edited by D. Henderson (Dekker, New York, 1992).